



An Advanced N -body Model for Interacting Multiple Stellar Systems

Miroslav Brož

Astronomical Institute of the Charles University, Faculty of Mathematics and Physics, V Holešovičkách 2, CZ-18000 Praha 8, Czech Republic
Received 2016 June 2; revised 2017 April 5; accepted 2017 May 7; published 2017 June 13

Abstract

We construct an advanced model for interacting multiple stellar systems in which we compute all trajectories with a numerical N -body integrator, namely the Bulirsch–Stoer from the *SWIFT* package. We can then derive various observables: astrometric positions, radial velocities, minima timings (TTVs), eclipse durations, interferometric visibilities, closure phases, synthetic spectra, spectral energy distribution, and even complete light curves. We use a modified version of the Wilson–Devinney code for the latter, in which the instantaneous true phase and inclination of the eclipsing binary are governed by the N -body integration. If all of these types of observations are at one’s disposal, a joint χ^2 metric and an optimization algorithm (a simplex or simulated annealing) allow one to search for a global minimum and construct very robust models of stellar systems. At the same time, our N -body model is free from artifacts that may arise if mutual gravitational interactions among all components are not self-consistently accounted for. Finally, we present a number of examples showing dynamical effects that can be studied with our code and we discuss how systematic errors may affect the results (and how to prevent this from happening).

Key words: binaries: close – binaries: eclipsing – methods: numerical – techniques: interferometric – techniques: photometric – techniques: radial velocities

1. Introduction

Traditional models of eclipsing binaries often have to account for additional external bodies, particularly a third light, which makes depths of primary and secondary minima shallower; a light-time effect, which causes periodic variations on O – C diagrams; a precession of the argument of periastron ω , which shifts the secondary minimum due to perturbations by the 3rd body; or changes of the inclination i with respect to the sky-plane, otherwise known as disappearing eclipses.

While analytical theories exist for descriptions of dynamical perturbations in triple stellar systems and corresponding transit timing variations (also known as TTVs, ETVs; see, e.g., Brown 1936; Harrington 1968; Söderhjelm 1975; Breiter & Vokrouhlický 2015; Borkovits et al. 2016), we prefer a more general approach—to account for *all* observational data; or at least as much as feasible. Thus, our aim is to incorporate astrometric or speckle-interferometric positions, radial velocities, minima timings, eclipse durations, spectro-interferometric visibilities, closure phases, synthetic spectra, spectral energy distribution, and light curves. At the same time, we do not want to be limited by inevitable approximations of the analytical theories (the N -body problem is not integrable) and the only way out seems to be an N -body integrator (as in Carter et al. 2011).

Another factor is that we cannot use analytical photometric models (like those used for exoplanet transits; Mandel & Agol 2002; Carter et al. 2008; Pál 2012) because the respective simplifications are not acceptable for stellar eclipses or for ellipsoidal variations outside eclipses.

In principle, our approach should be rather straightforward: we merge two codes into a single one; namely the Levison & Duncan (1994) *SWIFT* code, and the Wilson & Devinney (1971) WD code. In practice, a lot of work has to be done; because both of them have to be modified, we need to extract and derive observable quantities, read observational data, and check them by means of χ^2 statistics. Then, we need to run a minimization algorithm on top of them.

Even though we do not present new observational data here, there is one recent application of our N -body model to the ξ Tauri quadruple system that was described in a great amount of detail in Nemravová et al. (2016). Moreover, there is a comparison with a number of traditional, observation-specific models. In this “technical” paper, we prefer to show mostly results of numerical simulations, or even negative results contradicting the observations, to demonstrate the sensitivity of our model.

We have a few motivations to do so: (i) no complete and fully self-consistent N -body model currently exists that can account for all these observational constraints; (ii) we improved the model significantly compared to Nemravová et al., as we can now also fit complete light curves, and, optionally individual spectra (to be matched by synthetic ones); (iii) the previous paper was a bit lengthy and there was simply not enough room for a more technical description of our code; and (iv) we have to discuss the role of systematics, an experience gained during modeling of real multiple stellar systems.

2. Model Description

Let us begin with a description of the numerical integrator and the photometric model; then we present principal equations, a definition of the χ^2 metric used to compare the model with observational data, and a list of dynamical effects that can be modeled.

2.1. Numerical Integrator

We use the Bulirsch–Stoer numerical integrator (Press et al. 1999), with an adaptive time step, controlled by a unitless parameter ϵ_{BS} . The integrator sequentially divides the time step Δt by factors 2, 4, 6, ..., checks if the relative difference between successive divisions is less than ϵ_{BS} and then performs an extrapolation $\Delta t \rightarrow 0$ by means of a rational function (see Figure 1). If the maximum number of divisions $n_{\max} = 10$ is reached, the basic time step Δt has to be decreased, with

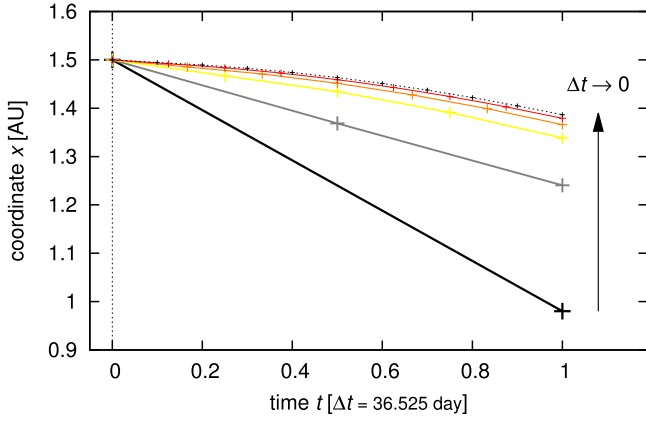


Figure 1. A principle of the Bulirsch–Stoer integrator. There is the time t as an independent variable on the abscissa and one of the coordinates x_b on the ordinate. A series of integrations with decreasing time steps $\Delta t_i = \frac{\Delta t}{2}, \frac{\Delta t}{4}, \frac{\Delta t}{6}, \dots$ is performed and then extrapolated for $\Delta t \rightarrow 0$ using a rational function. At the same time, relative differences between successive iterations have to be smaller than ϵ_{BS} .

another maximum number of trials $n_{try} = 30$. We recall this well-known principle here, as it is important to always understand the principles and limitations of the numerical methods in use. This kind of integrator is quite general and there are no restrictions for magnitudes of perturbations, so we can handle Keplerian orbits, tiny N -body perturbations, or even violent close encounters. Even though it is not symplectic, it does not suffer from an artificial periastron advance. On long timescales, it is worthwhile to check the energy conservation and eventually decrease ϵ_{BS} , perhaps down to 10^{-11} .

Apart from the internal time step, a user can choose the output time step Δt_{out} . The time stepping was adapted so that we first prepare a list of “times of interest” (corresponding to all observations) and the integrator outputs coordinates and velocities at exactly these times. Consequently, the need for additional interpolations is eliminated, except for minima timings and eclipse durations, where a linear interpolation from two close neighboring points separated by the expected duration is used, and optionally one can use binning for light curves (see below).

2.2. Photometric Model

The only restriction for the geometry of the stellar system is that only bodies 1 and 2 may be components of an eclipsing binary (or an ellipsoidal variable). Nevertheless, there can be any number of additional bodies, which do contribute to the total light, but we do not compute eclipses for them.

For light-curve computations, we use the WD 2005 version, in order to produce compatible and comparable results to Phoebe 1.0 (Prša & Zwitter 2005), but we plan to upgrade in the future. In brief, the WD code accounts for: blackbody radiation or the Kurucz atmospheres, bolometric limb-darkening, gravity-darkening, reflection, an axial rotation, or the Rossiter–McLaughlin effect. This is a relatively complex photometric model (more complex than analytical models of Mandel & Agol 2002; Carter et al. 2008). We use *no* spots or circumstellar clouds in this version. Usually, the code is called with mode 0 (no constraints on potentials) or 2 (the luminosity L_2 of the secondary is computed from the temperature T_2). Note that a number of parameters in the `lc.in` input file are useless (e.g., orbital elements, precession and period rates, luminosities, potentials etc.) because they are driven from elsewhere.

To speed up light-curve computations, we can use a binning of times Δt_{bin} and then linearly interpolate light-curve points to the times of observations. For high-cadence data, we can possibly gain a factor of 10 or 100 speed-up this way, but we have to be sure there is no physical process in our model that could change magnitudes on a timescale shorter than Δt_{bin} .

2.3. Principal Equations

Principal equations of our N -body model can be summarized as follows (the notation is described in Table 1): the equation of motion¹

$$\ddot{\mathbf{r}}_{bi} = - \sum_{j \neq i}^{N_{bod}} \frac{Gm_j}{r_{ji}^3} \mathbf{r}_{ji} + \mathbf{f}_{tidal} + \mathbf{f}_{oblat} + \mathbf{f}_{ppn}; \quad (1)$$

with the lowest-order tidal term (Hut 1981)

$$\mathbf{f}_{tidal} = - \sum_{j \neq i}^{N_{bod}} 3k_{Li} \frac{Gm_j^2}{m_i} \frac{R_i^5}{r_{ij}^8} \mathbf{r}_{ji}; \quad (2)$$

oblateness

$$\mathbf{f}_{oblat} = - \sum_{j \neq i}^{N_{bod}} \frac{1}{2} k_{Lj} \omega_{rotj}^2 \frac{R_j^5}{r_{ij}^5} \mathbf{r}_{ji}; \quad (3)$$

and parametrized post-Newtonian (PPN; Mardling & Lin 2002) terms

$$\mathbf{f}_{ppn} = - \sum_{j > i}^{N_{bod}} \frac{G(m_j + m_i)}{r_{ij}^2 c^2} \left\{ -2(2 - \eta_{ij}) \dot{r}_{ij} \dot{\mathbf{r}}_{ij} + \left[(1 + 3\eta_{ij}) \dot{\mathbf{r}}_{ij} \cdot \dot{\mathbf{r}}_{ij} - \frac{3}{2} \eta_{ij} \dot{r}_{ij}^2 - 2(2 + \eta_{ij}) \frac{G(m_j + m_i)}{r_{ij}} \right] \frac{\mathbf{r}_{ij}}{r_{ij}} \right\}. \quad (4)$$

Apart from trivial sky-plane positions x_{bi} , y_{bi} and radial velocities v_{zbi} , we can derive a number of dependent quantities, such as mid-eclipse timings (including light-time effects)

$$t'_{ecl} = t_{min} + \frac{z_{b1+2} - z_{b1+2}(t = T_0)}{c} - \frac{z_{h2}}{c}; \quad (5)$$

eclipse durations

$$\epsilon'_{ecl} = \frac{2}{\bar{v}_{h2}} \sqrt{(R_1 + R_2)^2 - \Delta_{min}^2}; \quad (6)$$

luminosities (alternatively, using a blackbody approximation, $\pi B_\lambda(T_{eff})$)

$$L_j(T_{effj}, R_j) = 4\pi R_j^2 \times \int_{\lambda - \Delta\lambda/2}^{\lambda + \Delta\lambda/2} F_{syn}(\lambda, T_{effj}, \log g_j, v_{rotj}, \mathcal{Z}_j) d\lambda; \quad (7)$$

¹ The program, including sources and example input data, is available at <http://sirrah.troja.mff.cuni.cz/~mira/xitau/>.

a limb-darkened complex visibility (Hanbury Brown et al. 1974;

$$\Theta = \pi\theta_j\sqrt{u^2 + v^2}, \quad \alpha = 1 - u_{\text{limb}}, \quad \beta = u_{\text{limb}}$$

$$V'(u, v) = \sum_{j=1}^{N_{\text{bod}}} \frac{L_j}{L_{\text{tot}}} \left(\frac{\alpha}{2} + \frac{\beta}{3} \right)^{-1} \times \left[\alpha \frac{J_1(\Theta)}{\Theta} + \beta \sqrt{\frac{\pi}{2}} \frac{J_{3/2}(\Theta)}{\Theta^{3/2}} \right] e^{-2\pi i (ux_{aj} + vy_{aj})}; \quad (8)$$

with $u_{\text{limb}}(\lambda, T_{\text{eff}j}, \log g_j, Z_j)$ interpolated from Van Hamme 1993); a complex triple-product

$$T_3' = V'(u_1, v_1)V'(u_2, v_2)V'(-u_1 - u_2, -(v_1 + v_2)); \quad (9)$$

the true phase of the eclipsing binary (at a time t modified by the light-time effects)

$$\varphi'_{\text{ecl}} = \frac{1}{2\pi} \arctan \frac{\hat{O} \cdot \hat{Y}}{\hat{O} \cdot \hat{X}}; \quad (10)$$

its inclination

$$i'_{\text{ecl}} = \arccos(-\hat{O} \cdot \hat{Z}); \quad (11)$$

Kopal potential (for the WD code that outputs relative magnitudes m'_V)

$$\Omega_{\text{Kopal}j} \doteq \left\langle \frac{1}{r_1} + \frac{q}{r_2} + \frac{1}{2}(1+q)r_3^2 \right\rangle_{\text{circle } \frac{R_j}{r_{12}}, \text{where}} \quad (12)$$

$$\mathbf{r}_1 \in \text{circle}, \quad \mathbf{r}_2 = \mathbf{r}_1 - (1, 0, 0), \quad \mathbf{r}_3 = \left(x_1 - \frac{q}{1+q}, y_1, 0 \right);$$

a normalized synthetic spectrum (with appropriate Doppler shifts)

$$I'_\lambda = \sum_{j=1}^{N_{\text{bod}}} \frac{L_j}{L_{\text{tot}}} I_{\text{syn}} \left[\lambda \left(1 - \frac{v_{z\text{bj}+\gamma}}{c} \right), T_{\text{eff}j}, \log g_j, v_{\text{rot}j}, Z_j \right]; \quad (13)$$

or a spectral energy distribution (in any of the *UBVRIJHK* bands)

$$F'_V = \sum_{j=1}^{N_{\text{bod}}} \left(\frac{R_j}{d} \right)^2 \int_0^\infty F_{\text{syn}}[\lambda, T_{\text{eff}j}, \log g_j, v_{\text{rot}j}, Z_j] f_V(\lambda) d\lambda, \quad (14)$$

where the component spectra (both I_{syn} and F_{syn}) can be either user-supplied or interpolated on-the-fly with Pyterpol (Nemravová et al. 2016) from AMBRE, POLLUX, BSTAR, OSTAR, or PHOENIX grids (Lanz & Hubený 2003, 2007; Palacios et al. 2010; de Laverny et al. 2012; Husser et al. 2013).

Internally, we use a barycentric left-handed Cartesian coordinate system with x negative in the right-ascension direction, y positive in declination, and z positive in radial, i.e., away from the observer; the units are day, au, au/day and au^3/day^2 for the time, coordinates, velocities, and masses, respectively. We also need additional coordinate systems, namely: Jacobian (for computations of hierarchical orbital elements), 1-centric (for an eclipse detection), 1 + 2 photocentric, or

Table 1

Notation Used for Coordinates, Velocities, and a Number of Other Quantities and Uncertainties That We Use in Our N -body Model

N_{bod}	number of bodies
m	mass (GM_\odot units)
$q = \frac{m_1}{m_2}$	mass ratio
$\eta_{ij} = \frac{m_j m_i}{(m_j + m_i)^2}$	symmetrized mass ratio
k_L	Love number
ω_{rot}	rotational angular velocity
x_b, y_b, z_b	barycentric coordinates
v_{xb}, v_{yb}, v_{zb}	barycentric velocities
x_h, y_h, z_h	1-centric coordinates
v_{xh}, v_{yh}, v_{zh}	1-centric velocities
x_p, y_p	1 + 2 photocentric sky-plane coordinates
x_{p3}, y_{p3}	1 + 2 + 3 photocentric coordinates
$x_a = \frac{x_h}{d}, y_a$	1-centric coordinates in an angular measure
$\hat{X}, \hat{Y}, \hat{Z}$	unit vectors aligned with 1 + 2 eclipsing pair
$\hat{O} = (0, 0, -1)$	observers direction
γ	systemic velocity
v_{rad}	observed radial velocity
t_{ecl}	mid-epoch of an eclipse of 1 + 2 pair
ϵ_{ecl}	eclipse duration
L, L_{tot}	component luminosity and the total one
T_{eff}	effective temperature
R	stellar radius
$\lambda, \Delta\lambda$	effective wavelength and bandwidth
$B_\lambda(T)$	the Planck function
V	complex visibility; squared visibility is $ V ^2$
T_3	complex triple-product; closure phase is $\arg T_3$
u, v	projected baselines (expressed in cycles, $\frac{B}{\lambda}$)
$\theta = \frac{2R}{d}$	angular diameter
u_{limb}	linear limb-darkening coefficient
d	distance to the system
m_V	magnitude (in V band or another)
m_0	zero-point
$I_\lambda, I_{\text{syn}}$	normalized monochromatic intensity
F_{syn}	absolute monochromatic flux (in $\text{erg s}^{-1} \text{cm}^{-2} \text{cm}^{-1}$)
$F_{V\text{calib}}$	calibration flux
f_V	filter transmission coefficient
$g = \frac{GM}{R^2}$	surface gravity, $\log g$ in cgs
v_{rot}	projected rotational velocity
Z	metallicity
$\sigma_{\text{sky major, minor}}$	uncertainty of the astrometric position,
	angular sizes of the uncertainty ellipse
ϕ_{ellipse}	position angle of the ellipse
$\mathbf{R}(\dots)$	the corresponding 2×2 rotation matrix
σ_{rv}	uncertainty of the radial velocity
σ_{tv}	uncertainty of the eclipse mid-epoch timing
σ_{ecl}	uncertainty of the eclipse duration
σ_{vis}	uncertainty of the squared visibility
σ_{clo}	uncertainty of the closure phase
σ_{t3}	uncertainty of the triple-product amplitude
σ_{lc}	uncertainty of the light-curve data
σ_{syn}	uncertainty of the normalized intensity
σ_{sed}	uncertainty of the spectral energy distribution
$m_j^{\text{min}}, m_j^{\text{max}}$	minimum and maximum masses

1 + 2 + 3 photocentric (for a comparison with astrometric observations of components 3 and 4).

One may immediately note a minor caveat of our model: the geometric radius (in Equation (6)), the effective radius (in Equation (7)), the limb-darkened radius (i.e., θ_j in Equation (8)), and the average radius (used in Equation (12)) are all assumed to be approximately the same. If this does not hold, it would be

necessary to add three more equations describing the relations between them.

2.4. Observational Data

When we compare our model with observations, we can compute χ^2 for astrometric positions, radial velocities, minima timings (TTVs), eclipse durations, interferometric squared visibilities, closure phases, triple-product amplitudes, light curves, synthetic spectra, and spectral energy distribution:

$$\chi^2 = \chi_{\text{sky}}^2 + \chi_{\text{rv}}^2 + \chi_{\text{ttv}}^2 + \chi_{\text{ecl}}^2 + \chi_{\text{vis}}^2 + \chi_{\text{clo}}^2 + \chi_{\text{t3}}^2 + \chi_{\text{lc}}^2 + \chi_{\text{syn}}^2 + \chi_{\text{sed}}^2 + \chi_{\text{mass}}^2, \quad (15)$$

where:

$$\chi_{\text{sky}}^2 = \sum_{j=1}^{N_{\text{bod}}} \sum_{i=1}^{N_{\text{sky } j}} \left\{ \frac{(\Delta x_{ji})^2}{\sigma_{\text{sky major } ji}^2} + \frac{(\Delta y_{ji})^2}{\sigma_{\text{sky minor } ji}^2} \right\}, \quad (16)$$

$$(\Delta x_{ji}, \Delta y_{ji}) = \mathbf{R} \left(-\phi_{\text{ellipse}} - \frac{\pi}{2} \right) \times \begin{pmatrix} x'_{pji} - x_{pji} \\ y'_{pji} - y_{pji} \end{pmatrix}, \quad (17)$$

$$\chi_{\text{rv}}^2 = \sum_{j=1}^{N_{\text{bod}}} \sum_{i=1}^{N_{\text{rv } j}} \frac{(v'_{zbi} + \gamma - v_{\text{rad } ji})^2}{\sigma_{\text{rv } ji}^2}, \quad (18)$$

$$\chi_{\text{ttv}}^2 = \sum_{i=1}^{N_{\text{ttv}}} \frac{(t'_{\text{ecl } i} - t_{\text{ecl } i})^2}{\sigma_{\text{ttv } i}^2}, \quad (19)$$

$$\chi_{\text{ecl}}^2 = \sum_{i=1}^{N_{\text{ecl}}} \frac{(\epsilon'_{\text{ecl } i} - \epsilon_{\text{ecl } i})^2}{\sigma_{\text{ecl } i}^2}, \quad (20)$$

$$\chi_{\text{vis}}^2 = \sum_{i=1}^{N_{\text{vis}}} \frac{(|V'(u_i, v_i)|^2 - |V_i|^2)^2}{\sigma_{\text{vis } i}^2}, \quad (21)$$

$$\chi_{\text{clo}}^2 = \sum_{i=1}^{N_{\text{clo}}} \frac{(\arg T'_{3i} - \arg T_{3i})^2}{\sigma_{\text{clo } i}^2}, \quad (22)$$

$$\chi_{\text{t3}}^2 = \sum_{i=1}^{N_{\text{t3}}} \frac{(|T'_{3i}| - |T_{3i}|)^2}{\sigma_{\text{t3 } i}^2}, \quad (23)$$

$$\chi_{\text{lc}}^2 = \sum_{k=1}^{N_{\text{band}}} \sum_{i=1}^{N_{\text{lc } k}} \frac{(m'_{Vki} + m_{0k} - m_{Vki})^2}{\sigma_{\text{lc } ki}^2}, \quad (24)$$

$$\chi_{\text{syn}}^2 = \sum_{i=1}^{N_{\text{syn}}} \frac{(I'_{\lambda i} - I_{\lambda i})^2}{\sigma_{\text{syn } i}^2}, \quad (25)$$

$$\chi_{\text{sed}}^2 = \sum_{i=1}^{N_{\text{sed}}} \frac{(m'_{Vi} - m_{Vi})^2}{\sigma_{\text{sed } i}^2}. \quad (26)$$

Again, the quantities are described in Table 1. The index i always corresponds to observational data, j corresponds to individual bodies, and k corresponds to sets of data. The primed quantities correspond to synthetic data, integrated (or interpolated) to the times of observations t_i .

We can also add an artificial term,

$$\chi_{\text{mass}}^2 = \sum_{j=1}^{N_{\text{bod}}} \left(\frac{2m_j - m_j^{\text{min}} - m_j^{\text{max}}}{m_j^{\text{max}} - m_j^{\text{min}}} \right)^{100}, \quad (27)$$

to keep the masses m_j of the components within reasonable intervals (e.g., according to spectroscopic classifications of

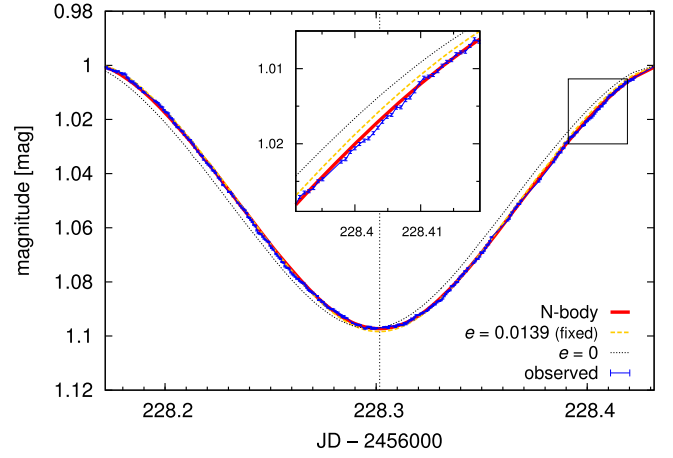


Figure 2. Light curves of a detached eclipsing binary and three dynamical models: (i) a Keplerian (two-body) assuming a fixed circular orbit ($e = 0$, black dotted line); (ii) a locally optimized Keplerian with a non-zero fixed eccentricity $e = 0.0139$ (yellow); and (iii) a full N -body model with the initial osculating $e_1(t = T_0) = 0$ (red), but with a general trajectory affected by perturbations among the four components. The last case corresponds to the arrangement of a ξ Tauri quadruple system (as described in Nemravová et al. 2016). The light curves and minima timings differ more than the usual uncertainty σ_{lc} , or σ_{ttv} , achievable by space-borne observations like that of *MOST* (Walker et al. 2003; cf. blue line with the tiny error bars; quasi-periodic oscillations were removed as explained in Appendix A.8). It is thus necessary to use the N -body model for such compact stellar systems, even on this very short (orbital) timescale.

the components). The high exponent of the arbitrary function prevents simplex from drifting away from the interval (m_j^{min} , m_j^{max}).

As usually, observational data have to be in a suitable format and we provide some example scripts for a conversion or extraction of data from OIFITS files (Pauls et al. 2005). Note that one should *not* use RV measurements when it is possible to fit the observed spectra with synthetic ones. Similarly, no minima timings or durations are needed when we have complete light curves available (cf. Figure 2); and no triple-product amplitudes $|T_3|$ are needed when the same interferometric measurements are used as squared visibilities $|V|^2$. We emphasize that it is always better to use directly observable quantities rather than derived ones.

To find a local or a global minimum, we can use a standard simplex algorithm or simulated annealing (Nelder & Mead 1965; Press et al. 1999), with the cooling schedule $T^{i+1} = (1 - \epsilon_{\text{temp}})T^i$, after a given number of iterations at T^i . Free parameters of the model (which can be optionally fixed) are: the masses m_j of the components, orbital elements a_j , e_j , i_j , Ω_j , ω_j , M_j of the respective orbits, systemic velocity γ , distance d , radii R_j , effective temperatures $T_{\text{eff } j}$, projected rotational velocities $v_{\text{rot } j}$, and magnitude zero-points m_{0k} . For N_{bod} bodies, this represents a set of $(10N_{\text{bod}} + N_{\text{band}} - 4)$ parameters in total.

Unfortunately, neither of the numerical methods can guarantee that the global minimum will be found. The multidimensional parameter space is very extended and there are many local minima, some of them statistically equivalent. Running simplex many times from different starting points (10^4 – 10^5) can help, but this problem is clearly both system-dependent and data-dependent. To obtain uncertainties of the

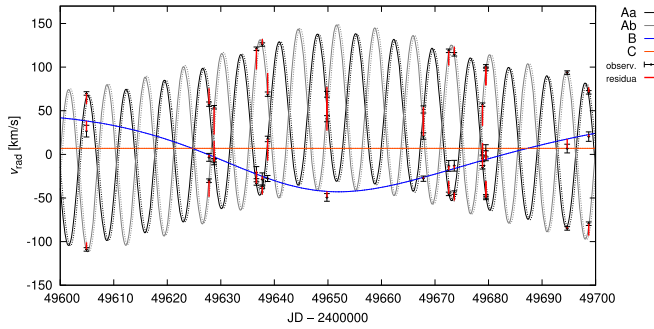


Figure 3. Evolution of radial velocities (RVs) of the four components of ξ Tauri (denoted Aa, Ab, B and C), assuming two different values of the initial osculating eccentricity $e_1(t = T_0)$ of the inner orbit: (i) zero (thick lines); (ii) an increased non-zero $e_1 = 0.01$ (dotted lines). There is a significant phase shift between them that can be easily detected because the respective RV measurements cover the interval of JD from 2449300 to 2456889. For even larger $e_1 \simeq 0.1$, the oscillations of RVs forced by the third body also have larger amplitude, related to the evolution of $e_1(t)$. For comparison, some of the observations are plotted (black points with error bars) along with residua with respect to the worse non-zero e_1 model (red lines).

model parameters or a full covariance matrix, one can use the bootstrap method (Efron 1979), for example.

2.5. Dynamical Effects

A number of well-known dynamical effects can be modeled with the N -body integrator: self-consistent precession of ω and Ω , inclination changes and eclipse durations, eccentricity oscillations (Figure 3), Kozai cycles, variation and evection, differences between prograde versus retrograde orbits, close encounters, hyperbolic trajectories, mean-motion resonances (Rivera et al. 2005), secular resonances, three-body resonances (Nesvorný & Morbidelli 1998), or chaotic diffusion due to overlapping resonances, which are also naturally accounted for in our N -body model. Even more examples can be found in Fabrycky (2010).

3. Model Testing

3.1. A Test on Synthetic Data

In order to test a basic functionality of our N -body model, we created a mock system with 40 known parameters; the system actually closely corresponds to the quadruple star ξ Tau (see Table 2). Synthetic observational data were created using the same code with the same coverage and cadence as the real observations of ξ Tau (Nemravová et al. 2016): 78,133 spectral measurements (individual data points $I_{\lambda i}$), 17 391 squared visibilities $|V_i|^2$, 4 856 complex triple products $T_{3 i}$, 2 974 light-curve points m_{Vki} , 17 astrometric measurements Δx_{ij} , Δy_{ij} of the 4th component, and 13 SED points m_{Vj} . A Gaussian noise was applied to all of them, at levels typical for the data sets we have for ξ Tau; and we assumed there are *no* systematics, neither in these synthetic observations, nor in the model (but cf. Appendices A.3–A.8). For the true solution, one would obtain $\chi^2 = 109,095$, which is indeed a perfect solution given the number of degrees of freedom $\nu \equiv N_{\text{data}} - M_{\text{free}} = 108,257 - 40 = 108,217$, and the probability $P(\chi^2|\nu) = 0.970$ that the χ^2 value is that large by chance.

We then performed several simplex optimizations, starting from a number of neighboring points, farther and farther away

from the true solution. The convergence of the simplex to a local minimum is clear (Figure 4) and we recovered the original parameters (low $\chi^2 \simeq \nu$) with some uncertainties, as expected; unless the initial guess was too far away, say, more than a few percent of the critical parameters (see Figure 5). More extended surveys with many initial starting points and/or simulated annealing would be needed in these unfortunate cases. The differences between the final and true solutions roughly correspond to the uncertainties we would obtain from bootstrap testing.

Often some preliminary knowledge based on observation-specific models is available (e.g., prominent periods, previously published parameters). The N -body model is especially suitable for such “semi-final” convergence—with all parameters free—which should limit the systematics arising from the usage of limited (Keplerian) models.

Regarding the fractional or missing data, there are several rather trivial facts, e.g., if we miss RVs, it is impossible to resolve low- e orbits from high- e with $\omega = 0^\circ$ or 180° . If there are no eclipses and no interferometric measurements available, one cannot precisely constrain the inclination i . Without closure phase measurements, there is practically no sensitivity to asymmetries, etc. Of course, they are interesting when dealing with real observational data sets (see also Appendix A.2).

Let us point out that this kind of testing has somewhat limited capabilities. First, if we create the mock data with the same model, then this test is essentially a test of the numerical methods (simplex and simulated annealing). Because these methods are indeed classical (Nelder & Mead 1965), their limitations are already very well known.

Second, to create the mock data independently, one would need a completely independent model with exactly the same capabilities. However, this is a test of systematic differences between the models rather than a test of the method itself. We consider this approach to be more useful, but it is rather difficult to obtain the second model. Of course, any Keplerian models (e.g., Phoebe 1.0) are useless. Any model that does not produce all the observables (astrometry, RVs, TTVs, e_{ecl} , $|V|^2$, T_3 , m_V , or I_λ) is impractical too, because we need as many orthogonal constraints as possible. Analytical photometric models (e.g., Carter et al. 2008) are too simplified for stellar binaries. And so on. It may be possible to use Phoebe 2.0 (Prša et al. 2016) for a such comparison in the future.

Finally, real observational data of real systems have their own cadence, coverage, calibrations, uncertainties, and systematics. Even though one can play with artificial data, these tests cannot be used straightforwardly, because we know “nothing” a priori about the given data we obtain from observers. Consequently, one will have to perform suitable tests again and again for every subsequent system.

3.2. A Comparison with Other Models

As already mentioned in the Introduction, a comparison with several observation-specific models was already done in our previous paper (Nemravová et al. 2016). In particular, our N -body model produces results that are compatible *within* respective approximations (e.g., on short timescales when the Keplerian model can be regarded as a useful approximation) with the following published works: the photometric model of Phoebe 1.0 (Prša & Zwitter 2006); the astrometric and speckle-interferometry

Table 2
The Mock System Parameters That Were Used to Generate Synthetic Data for Testing

Par.	Value							Unit
m_1	2.238483	m_2	2.009645	m_3	3.7472	m_4	0.92	M_\odot
a_1	0.1176356	a_2	1.08420	a_3	28.39	au
e_1	0.0000	e_2	0.2167	e_3	0.568
i_1	87.6	i_2	86.3	i_3	-18.2	deg
Ω_1	329.1	Ω_2	328.6	Ω_3	114.7	deg
ω_1	275.65	ω_2	0.00	ω_3	1.0	deg
M_1	174.44	M_2	88.04	M_3	32.7	deg
γ	8.82	km s ⁻¹
d	67.9	pc
T_{eff1}	10727	T_{eff2}	10275	T_{eff3}	13120	T_{eff4}	6526	K
R_1	1.586	R_2	1.642	R_3	2.727	R_4	0.877	R_\odot
v_{rot1}	16.2	v_{rot2}	12.5	v_{rot3}	234.9	v_{rot4}	80.1	km s ⁻¹
m_{01}	1.000	m_{02}	3.335	m_{03}	3.646	m_{04}	3.730	mag

Note. The notation is the same as in Table 1. Values rounded to typical uncertainties of the parameters are presented in this table. The osculating elements correspond to the epoch $T_0 = 2,456,224.724705$.

model of Zasche & Wolf (2007); the RV disentangling by Korel (Hadrava 1997); the LitPro model for visibilities $|V|^2$ (Tallon-Bosc et al. 2008); the spectro-interferometric $|V|^2$ and T_3 (Nemravová et al. 2016); and the synthetic spectra fitting by Pyterpol (dtto).

4. Conclusions and Future Work

Today, N -body models seem to be an absolutely necessary tool for a careful inspection of observational data. It is important to take care that discrepancies between Keplerian and full N -body dynamics no longer spoil derived stellar parameters. After a removal of (some) systematic errors (sometimes) present in observations or reductions, N -body models enable us to reveal even tiny N -body perturbations and construct robust models of compact stellar systems (e.g., those from Table 3).

Regarding future developments of (our or other) N -body models, it seems worthwhile to also account for: calibration factors of individual interferometric telescopes, gravity-darkening in the visibility calculation of rotating stars (as in Aufdenberg et al. 2006), especially when measuring on the longest baselines, and eventually one may think of an upgrade to the WD 2015, or Phoebe 2.0 (already used in Pablo et al. 2015).

Yet another work is needed to compute trajectories even more accurately, with physics going beyond point-like masses, equilibrium tides or oblateness, namely the following: higher gravitational moments (J_4) due to the non-sphericity of stellar components, tidal dissipation and cross-tides (e.g., Mignard 1979), corresponding long-term evolution of orbits, spin evolution (Eggleton & Kiseleva-Eggleton 2001), spin-orbital resonances, or radiation of gravitational waves in extreme cases.

The situation in stellar interiors also matters. The dissipation occurs either because of viscosity in outer convective zones, or inertial oscillations in radiative zones, which are excited on eccentric orbits by dynamic tides and subsequently radiatively damped (Zahn 2008). In triple systems, the excitations may actually arise from a binary subsystem, and corresponding light oscillations then have half of its period (Derekas et al. 2011; Fuller et al. 2013). Another difficulty stems from certain coupling of envelopes and cores (Papaloizou & Ivanov 2010). Inevitably, a fully self-consistent model should account for a

back-reaction: the strongest tidal heating may inflate whole objects (Mardling 2007).

The work of M.B. was supported by the grants no. P209-15-02112S and P209-13-01308S of the Czech Science Foundation. I thank Jana Nemravová and David Vokrouhlický for valuable discussions on the subject and a fruitful collaboration on the ξ Tauri paper. I also have to thank the referee Hagai Perets for constructive criticism that determined the final structure of the paper.

Appendix A Possible Problems due to Systematics

We have to admit that any modeling (compact stellar systems included) can be spoiled, either when there are systematic deficiencies of the model, e.g., Keplerian versus N -body, or serious systematic errors in observational data, especially when we use very heterogeneous data sets. In the following, we thus discuss several “dangerous” cases.

A.1. Discretization Errors

Of course, any numerical computation suffers from discretization errors and interpolation errors, even though we tried to decrease the latter as much as possible (cf. Section 2). This is probably the most important disadvantage compared to analytical computations. A general rule is a convergence of results (and corresponding χ^2 values) for $\Delta t \rightarrow 0$.

However, let us add the warning that rarely, a decrease of the time step, e.g., by a factor of 2, may lead to unexpected results. For example, when eclipses are almost disappearing, the trajectory with $\Delta t/2$ is more curved and may thus miss the last eclipse, which suddenly *increases* χ_{tiv}^2 because the next eclipse is now one orbital period P far away. The solution is to converge the model once again, with $\Delta t/2$.

Also, there is yet another discretization related to the WD code, or the surfaces of the eclipsing binary. For low numbers N_{wd} , one can see numerical artifacts on the light curve, as rectangular surface facets appear from behind the limb, or disappear. Again, it is worthwhile to check larger N_{wd} .

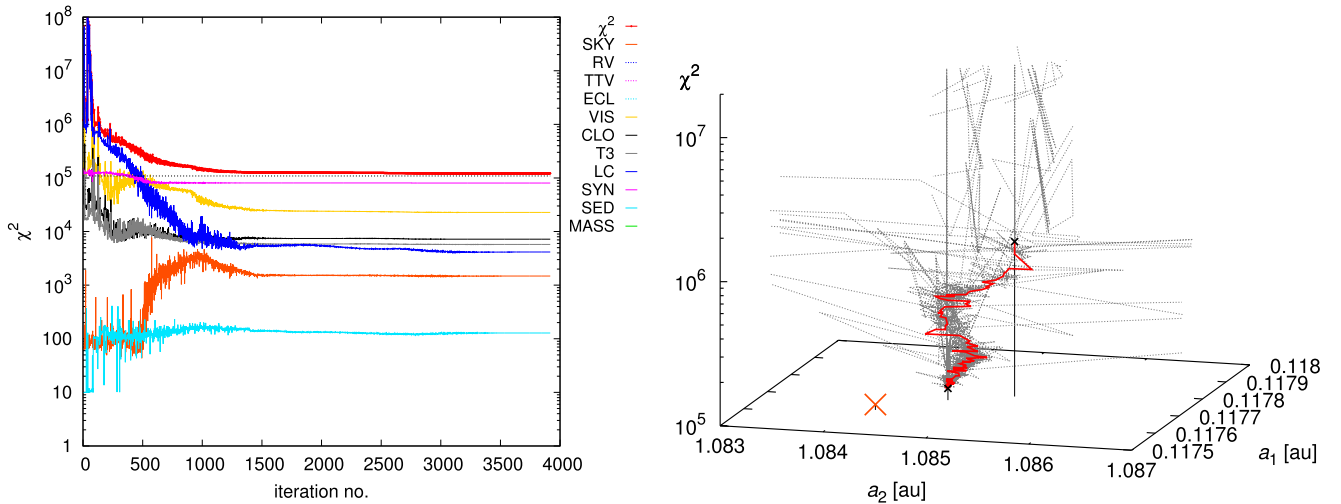


Figure 4. Left: a convergence of the simplex to a local minimum vs. the number of iterations for the mock system from Table 2. Individual contributions to the total χ^2 corresponding to Equation (15) are shown. Initially, all of the 40 parameters were shifted by 0.1% and the χ^2 value suddenly increased up to 1.19×10^7 because the model is very sensitive to some of them. The final value after $\simeq 10^3$ iterations is $\chi^2 = 120\,625$. This is quite close to the true solution, but still some restarts of the simplex (or simulated annealing) would be needed to obtain a χ^2 as low as 109 095, i.e., the value of the true solution (albeit with noisy synthetic data). Moreover, iterations with increased weights w_{sky} and w_{sed} would also be needed. The convergence of χ^2 with respect to semimajor axes a_1, a_2 (i.e., 2 out of 40 free parameters). One may see the initial (offset) and final positions (black crosses), successful steps (red solid lines), unsuccessful trials (gray dotted), and the true solution (orange cross). While the simplex approaches the true solution, it is often stuck halfway in a local minimum.

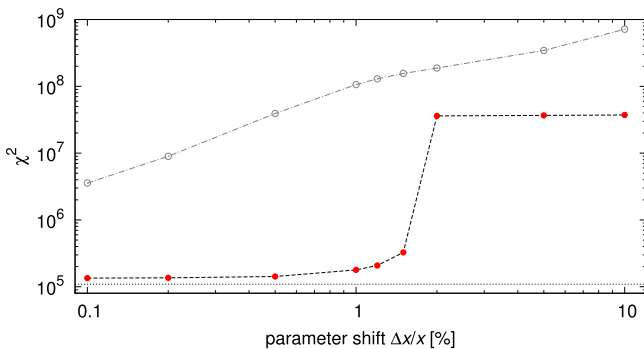


Figure 5. Final χ^2 values (filled circles) after $\simeq 10^3$ simplex iterations vs. relative shifts of the initial parameters (expressed in percentages). For comparison, there are also initial χ^2 's (open circles) we started simplex at. The true solution reference value is $\chi^2 = 109,095$ (dotted line). For the purpose of this test, we used osculating periods P_i as fixed (and unshifted) parameters, instead of free semimajor axes a_i , as they are usually well constrained by period analyses. We also kept a_j fixed $T_{\text{eff},j}$, $v_{\text{rot},j}$ and used simple bandpasses and Planck approximation to speed-up computations.

A.2. Mirror Solutions

Quite often, we can expect one or more (m) mirror solutions (and 2^m combinations of them). A typical situation is that we have no RVs for faint components (so that both inclinations i and $i' = -i$ are admissible), or no unambiguous astrometry or closure-phase measurements (so that Ω and $\Omega' = 180^\circ - \Omega$ are both admissible). Consequently, one may save some time when surveying the parameter space.

However, with the N -body model at hand it is worthwhile to check not only the total χ^2 but also *individual contributions* to χ^2 for all the mirror models. In particular, χ_{ttv}^2 is very sensitive to the mutual perturbations, and we may be able to resolve some of the ambiguities mentioned above.

Of course, the statistics must not be corrupted by systematics or strongly underestimated uncertainties in other observational data sets. If this is the unfortunate case, one may try to use

Table 3

Suggested Examples of Compact Stellar Systems for Which the N -body Model Could Be Useful (or Inevitable)

Designation	Reference
λ Tau	Fekel & Tomkin (1982)
ξ Tau	Nemravová et al. (2016)
VW LMi	Pribulla et al. (2008)
V994 Her = HD 170314	Zasche & Uhlář (2016)
V907 Sco = HD 163302	Lacy et al. (1999)
HD 91962	Tokovinin et al. (2015)
HD 109648	Jha et al. (2000)
HD 144548	Alonso et al. (2015)
HD 181068 = KIC 5952403	Fuller et al. (2013)
KIC 05255552	Borkovits et al. (2016)
KIC 05771589	...
KIC 06964043	...
KIC 07289157	...
KIC 07668648	...
KIC 07955301	...
KIC 09714358	...

Note. This “catalog” obviously cannot be considered comprehensive.

weights w of individual χ^2 's, but this should be used as “a method of last resort.” The reason is that it is too easy to hide *all* systematics this way, even though it is better to get rid of them (see below).

A.3. Heterogeneous Data Sets of RVs

Radial-velocity measurements might be affected by zero-point offsets, which then lead to different systemic velocities γ for different observatories. This can be a bit misleading because it is not possible to a priori distinguish systematic differences in dispersion relations from real perturbations, when the observations were acquired at epochs distant in time.

A well-known viable approach is to use an independent calibration by narrow interstellar lines (DIBs; Chini et al. 2012), if they are present and resolved in the given

spectral range. Another possibility is atmospheric lines for which the relative RVs can be computed easily. If this is impossible, one should use the N -body model with great caution, because simply increasing $\sigma_{rv} \simeq \Delta\gamma$ to get $\chi_{rv}^2 \simeq N_{rv}$ is the wrong approach. The RV measurements in question will still “push” the model elsewhere and there will be systematic departures with respect to other (more or less orthogonal) observational data.

It may be too much freedom, but if the dispersion relations can be considered stable from night to night, some calibration factors $f_{rv,k}$ of RVs—assigned to individual observatories or data sets—might actually be a better solution. In any case, such factors have to always be treated as additional free parameters of the N -body model.

A.4. RVs from Disentangling

Sometimes, RVs are derived in the Fourier domain by means of disentangling (e.g., by Korel; Hadrava 1995), with the advantage that one obtains disentangled spectra of individual components. There is a “hidden” caveat, though, because one can expect a strong correlation of RVs and the fixed Keplerian orbital elements used during the disentangling procedure. This is a problem because we vary initial osculating orbital elements in the N -body model and they most likely will contradict the previous elements.

Note that the disentangled spectra should *not* be re-used as templates, because they contain slight systematic asymmetries or wavy continua. If we try to match the observed spectra with such templates again, we will obtain artificially small uncertainties σ_{rv} (and extremely large χ_{rv}^2). A solution is to use synthetic spectra similar to the disentangled ones, but with no direct relation to Korel, as an intermediate step to derive new RVs.

A.5. RVs from Synthetic Spectra

Alternatively, RVs of the individual components can be derived directly in the time domain by fitting a luminosity-weighted sum of suitable synthetic spectra (e.g., by Pyterpol; Nemravová et al. 2016). Instead of fitting the observed spectra individually (one-by-one), it is advisable to assume that most of the free parameters (projected $v_{rot,j}$, $T_{eff,j}$, gravity $\log g_j$, and metallicity Z_j of the stellar components) are the same for all spectra, with the exception of RVs that are surely time-dependent. Luckily, these RVs are *not* strongly correlated with the orbital elements, so they seem suitable as an input for the N -body model.

On the other hand, this method can have problems of its own when RVs are small (at conjunctions) and v_{rot} is large, which causes the lines to be totally blended. As a provisional solution, one may try to discard the lowest RVs that cause the problems, or *not* use RVs at all and instead fit synthetic spectra directly with the N -body model (χ_{syn}^2), which is definitely a better approach, because RVs will be correctly tied to each other (see Figure 6).

A.6. Rectification Procedure

Inevitably, RVs might have been systematically affected already during a basic reduction, namely a rectification (normalization) of spectra. If the rectification procedure is automated by fitting a low-degree polynomial to continua, it is

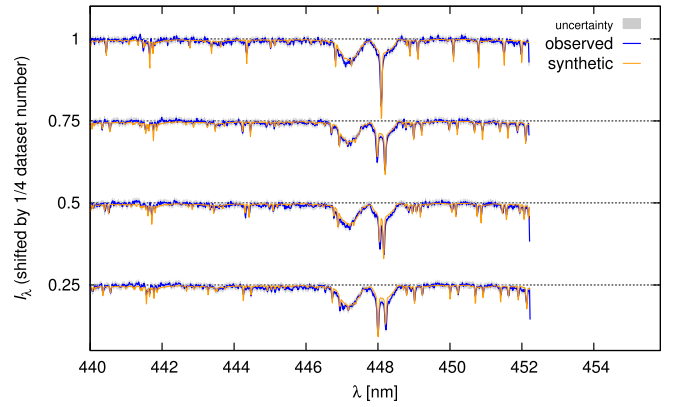


Figure 6. A small subset of the observed spectra of ξ Tauri (blue), fitted by a triplet of synthetic spectra (orange) for components Aa, Ab (sharp-lined), and B (broad-lined). The Doppler shifts were set according to the N -body model; consequently, there is no problem with the blending of lines in the top spectrum. The respective parameters of the components were assumed as follows: the effective temperature $T_{eff} = 10,700, 10,480, 14,190$ K; surface gravity $\log g = 4.08, 4.01, 4.527$; projected rotational velocity $v_{rot} = 12.6, 14.3, 229.2$ km s $^{-1}$; and the metallicity was solar. The relative luminosities were $L = 0.203, 0.134, 0.644 L_{\odot}$, while the component C was considered too faint. The synthetic spectra were prepared with Pyterpol (Nemravová et al. 2016).

worthwhile to try a different maximum degree of the polynomial and run the above synthetic spectra optimization once again.

A.7. Visibility Calibration

Contrary to closure phase arg T_3 measurements, the squared visibility $|V|^2$ has to be calibrated by close-in-time observations of comparison stars with known angular diameters or unresolved (point-like) sources. Sometimes, even the calibrated measurements exhibit unrealistically quick changes of $|V|^2$ or sudden decreases of $|V|^2$, possibly caused by unfavorable weather conditions, or seeing comparable to the slit width, affecting a light contribution from barely resolved components, or other obscure instrumental defects.

In the end, dropping these suspicious observational data may be the only way to prevent the systematics to unrealistically shift the model. Using a low weight $w_{vis} = 0.1$ is not a satisfactory option. To this point, we always retain a data set identification for each single measurement that enables us to quickly perform a bootstrap testing.

A.8. Quasi-periodic Oscillations

A removal of quasi-periodic light oscillations that are sometimes present (or always for high-precision measurements) outside eclipses is very important, because they may otherwise systematically offset the minima timings themselves. One wave of the oscillations behaves like a “ramp,” which skews the light curve around the minimum.

The observed light curve should thus be *locally* fitted by a suitable function (e.g., harmonic with a variable period and amplitude) and then subtracted from the data. If the (synthetic) light curve out of eclipses is flat beyond doubt, it seems better to drop these segments of the (observed) light curve completely, because they would increase χ_{lc}^2 ; but there is no

useful information, as we have no physical model for these oscillations (yet).

A.9. Osculating versus Fixed Elements

Some care is also needed when comparing results of (old) Keplerian and (new) N -body models. They actually *can* differ by more than a few σ , because the former orbital elements are fixed, while the latter are only osculating initial conditions at $t = T_0$. Generally, all elements are time-dependent quantities, $a_1(t)$, $e_1(t)$, $i_1(t)$, etc., whereas their oscillations are often *larger* than the uncertainties of the initial osculating elements. In fact, one can perform some averaging over the observational time span to facilitate the comparison. Nevertheless, the N -body model is more complete, and it should be probably preferred.

A.10. Stability, Aliasing, Mean, and Proper Elements

It is also possible to run the N -body integrator separately, regardless of an observational time span, and study the long-term evolution and stability of stellar systems. We may wish to prefer those orbital solutions that are indeed stable. One of the difficulties is that the output of osculating elements is either prohibitively long or an *aliasing* occurs when the output time step Δt_{out} is larger than half of the shortest orbital period, $P_1/2$.

In a modified version of the BS integrator (`swift_bs_fp`), we can use an online digital filtering of non-singular osculating elements h_j , k_j , p_j , q_j to overcome these problems: first a multi-level convolution based on the Kaiser windows (Quinn et al. 1991) to obtain *mean* elements, and second a frequency-modified Fourier transform (Šidlichovský & Nesvorný 1996) to extract *proper* elements. For N mutually interacting bodies, one can expect $2N$ eigenfrequencies of the system, which are usually denoted g_j and s_j . The corresponding amplitudes e_{pj} , $\sin \frac{1}{2}i_{pj}$ can be considered approximate integrals of motion that only evolve on timescales longer than secular.

To conclude pessimistically, the above list of possible problems and systematics cannot be treated as complete, unfortunately.

Appendix B Technical Notes

B.1. Different Hierarchy

By default, we assume a hierarchy of $((1 + 2) + 3) + 4$, for which Jacobian orbital elements seem to be a suitable description. For a substantially different hierarchy, say, two pairs $(1 + 2)$ and $(3 + 4)$, where we would prefer a different definition of elements, only a very small part of the code has to be rewritten, namely in the `geometry.f` subroutine, where the elements are converted to barycentric Cartesian coordinates. Alternatively, one may wish to use 1-centric Cartesian coordinates as actual parameters, because sometimes precise observational data may constrain (“fix”) some of them (x_{h2} , y_{h2} , etc.), thus decreasing the dimensionality of the parameter space.

B.2. Jacobian Orbital Elements

Unlike the usual stellar-astronomy convention, where the brightest component is always at the origin of the reference frame, in our N -body model we usually select the most compact

eclipsing pair as bodies 1 and 2, or the most massive component as 1. The reason is that orbital elements in hierarchical systems are usually computed in Jacobian coordinates, where the center of mass $1 + 2$ is the reference point for the coordinates and velocities of the third body; the $1 + 2 + 3$ center of mass is a suitable reference for the fourth body, and so on. The corresponding Jacobian elements then have a nice interpretation. Because of the above definition, it may be necessary to adjust to-be-fitted astrometric measurements by 180° in the position angle—not due to an ambiguity, but simply because the reference body is different in our case. Similarly, a value of Ω from the literature may actually differ by 180° .

References

- Alonso, R., Deeg, H. J., Hoyer, S., et al. 2015, *A&A*, **584**, L8
 Aufdenberg, J. P., Mérand, A., Coudé du Foresto, V., et al. 2006, *ApJ*, **645**, 664
 Borkovits, T., Hajdu, T., Sztakovics, J., et al. 2016, *MNRAS*, **455**, 4136
 Breiter, S., & Vokrouhlický, D. 2015, *MNRAS*, **449**, 1691
 Brown, E. W. 1936, *MNRAS*, **97**, 56
 Carter, J. A., Fabrycky, D. C., Ragozzine, D., et al. 2011, *Sci*, **331**, 562
 Carter, J. A., Yee, J. C., Eastman, J., et al. 2008, *ApJ*, **689**, 499
 Chini, R., Hoffmeister, V. H., Nasserri, A., et al. 2012, *MNRAS*, **424**, 1925
 de Laverny, P., Recio-Blanco, A., Worley, C. C., & Plez, B. 2012, *A&A*, **544**, A126
 Derekas, A., Kiss, L. L., Borkovits, T., et al. 2011, *Sci*, **332**, 216
 Efron, B. 1979, *AnSta*, **7**, 1
 Eggleton, P. P., & Kiseleva-Eggleton, L. 2001, *ApJ*, **562**, 1012
 Fabrycky, D. C. 2010, in *Exoplanets*, ed. S. Seager (Tucson, AZ: Univ. Arizona Press), 217
 Fekel, F. C., & Tomkin, J. 1982, *ApJ*, **263**, 289
 Fitzpatrick, R. 2012, *An Introduction to Celestial Mechanics* (Cambridge: Cambridge Univ. Press)
 Fuller, J., Derekas, A., Borkovits, T., et al. 2013, *MNRAS*, **429**, 2425
 Hadrava, P. 1995, *A&AS*, **114**, 393
 Hadrava, P. 1997, *A&AS*, **122**, 581
 Hanbury Brown, R., Davis, J., Lake, R. J. W., & Thomson, R. J. 1974, *MNRAS*, **167**, 475
 Harrington, R. S. 1968, *MNRAS*, **AJ**, **73**, 190
 Husser, T.-O., Wende-von Berg, S., Dreizler, S., et al. 2013, *A&A*, **553**, A6
 Hut, P. 1981, *A&A*, **99**, 126
 Jha, S., Torres, G., Stefanik, R. P., Latham, D. W., & Mazeh, T. 2000, *MNRAS*, **317**, 375
 Kozai, I. 1962, *AJ*, **67**, 591
 Lacy, C. H. S., Helt, B. E., & Vaz, L. P. R. 1999, *AJ*, **117**, 541
 Lanz, T., & Hubený, I. 2003, *ApJS*, **146**, 417
 Lanz, T., & Hubený, I. 2007, *ApJS*, **169**, 83
 Levison, H. F., & Duncan, M. J. 1994, *Icar*, **108**, 18
 Lidov, M. L. 1962, *P&SS*, **9**, 719
 Mandel, K., & Agol, E. 2002, *ApJ*, **580**, 171
 Mardling, R. A. 2007, *MNRAS*, **382**, 1768
 Mardling, R. A., & Lin, D. N. C. 2002, *ApJ*, **573**, 829
 Mardling, R. A., & Lin, D. N. C. 2004, *ApJ*, **614**, 995
 Mignard, F. 1979, *M&P*, **20**, 301
 Nelder, J. A., & Mead, R. 1965, *CompJ*, **7**, 308
 Nemravová, J., Harmanec, P., Brož, M., et al. 2016, *A&A*, **594**, 55
 Nesvorný, D., & Morbidelli, A. 1998, *AJ*, **116**, 3029
 Pablo, H., Richardson, N. D., Moffat, A. F. J., et al. 2015, *ApJ*, **809**, 134
 Pál, A. 2012, *MNRAS*, **420**, 1630
 Palacios, A., Gebran, M., Josselin, E., et al. 2010, *A&A*, **516**, A13
 Papaloizou, J. C. B., & Ivanov, P. B. 2010, *MNRAS*, **407**, 1631
 Pauls, T. A., Young, J. S., Cotton, W. D., & Monnier, J. D. 2005, *PASP*, **117**, 1255
 Press, W. H., Teukolsky, S. A., Vetterlink, W. T., & Flannery, B. P. 1999, *Numerical Recipes in Fortran* (Cambridge: Cambridge Univ. Press), 77
 Pribulla, T., Baluđanský, D., Dubovský, P., et al. 2008, *MNRAS*, **390**, 798
 Prša, A., Conroy, K. E., Horvat, M., et al. 2016, *ApJS*, **227**, 29
 Prša, A., & Zwitter, T. 2005, *ApJ*, **628**, 426
 Prša, A., & Zwitter, T. 2006, *ApJS*, **304**, 347

- Quinn, T. R., Tremaine, S., & Duncan, M. 1991, *AJ*, **101**, 2287
- Rivera, E. J., Lissauer, J. J., Butler, R. P., et al. 2005, *ApJ*, **634**, 625
- Söderhjelm, S. 1975, *A&A*, **42**, 229
- Šidlichovský, M., & Nesvorný, D. 1996, *CeMDA*, **65**, 137
- Tallon-Bosc, I., Tallon, M., Thibaut, E., et al. 2008, *Proc. SPIE*, **7013**, 70131J
- Tokovinin, A., Latham, D. W., & Mason, B. D. 2015, *AJ*, **149**, 195
- Tokovinin, A. A. 1986, *ATsir*, **1415**, 1
- Van Hamme, W. 1993, *AJ*, **106**, 2096
- Walker, G., Matthews, J., Kuschnig, R., et al. 2003, *PASP*, **115**, 1023
- Wilson, R. E., & Devinney, E. J. 1971, *ApJ*, **166**, 605
- Zahn, J.-P. 2008, in *EAS Publ. Ser.* 29, 67
- Zasche, P., & Uhlář, R. 2016, *A&A*, **588**, 121
- Zasche, P., & Wolf, M. 2007, *AN*, **328**, 928